Competition of rotation around the intermediate and long axes in ^{193}Tl

J. Ndayishimye,[1,2] E. A. Lawrie,[1,3,*] O. Shirinda,[1,2] J. L. Easton,[1,3] J. J. Lawrie,[1] S. M. Wyngaardt,[2] R. A. Bark,[1] T. D. Bucher,[1,2] S. P. Bvumbi,[4] T. R. S. Dinoko,[5] P. Jones,[1] N. Y. Kheswa,[1] S. N. T. Majola,[1,4,6] P. L. Masiteng,[4] D. Negi,[1] J. N. Orce,[3] J. F. Sharpey-Schafer,[3] and M. Wiedeking[1]

[1]*iThemba LABS, National Research Foundation, P.O. Box 722, 7129 Somerset West, South Africa*
[2]*Department of Physics, University of Stellenbosch, Private Bag X1, 7602 Matieland, South Africa*
[3]*Department of Physics, University of the Western Cape, Private Bag X17, 7535 Bellville, South Africa*
[4]*Department of Physics, University of Johannesburg, P.O. Box 524, 2006 Auckland Park, South Africa*
[5]*Radio Frequency Metrology, National Metrology Institute, Private Bag X34, Lynnwood Ridge, 0040 Pretoria, South Africa*
[6]*Department of Physics, University of Zululand, Private Bag X1001, KwaDlangezwa 3886, South Africa*

(Received 11 April 2019; published 19 July 2019)

High-spin states in ^{193}Tl were studied and the level scheme was revised and extended including the observation of new rotational bands. A surprising competition between bands built on the same $\pi h_{9/2} \otimes \nu i_{13/2}{}^{-2}$ nucleon configurations is observed. It is suggested that it is generated by two different rotational modes of this triaxial nucleus: (i) a rotation around the intermediate nuclear axis, producing a pair of chiral symmetry bands, and (ii) a rotation around the long nuclear axis, producing a third band with lower alignment.

DOI: 10.1103/PhysRevC.100.014313

I. INTRODUCTION

Triaxial nuclei may exhibit chiral symmetry in angular momentum space [1]. A nonplanar system is built of three angular momenta—those of the core and of the odd nucleons with particle and hole nature—which align along the three major axes of the nucleus. These three angular momenta can be arranged into a left- or a right-handed system, therefore they form a chiral object. Chiral symmetry is exhibited by a pair of near-degenerate $\Delta I = 1$ rotational bands. So far a number of chiral candidates were observed in nuclei located in four mass regions: $A \approx 80$, 100, 130, and 190 [2–52]. The chiral systems in the Tl isotopes, in particular those built on the $\pi h_{9/2} \otimes \nu i_{13/2}{}^{-n}$ configurations (where $n = 1, 2, 3$) are very unusual, as they show a competition of several bands built on the same configuration. Two Tl isotopes, ^{194,195}Tl are studied up to high spins, where three- and four-quasiparticle systems form [23–25,53]. In ^{195}Tl only results on chiral pairs have been published to date [53], but in ^{194}Tl the two chiral partner bands built on the $\pi h_{9/2} \otimes \nu i_{13/2}{}^{-3}$ configuration compete with another rotational band built on the same $\pi h_{9/2} \otimes \nu i_{13/2}{}^{-3}$ configuration [24]. This competition is difficult to understand. For instance, do these bands correspond to the same triaxial deformation? If they do, we should observe two chiral systems, generating two pairs of partner bands. Multiple chiral systems can indeed form in a single nucleus, as theoretical calculations show (e.g., [15,44,54–62]) and as experimental data suggest (e.g., [53,63–67]). Alternatively, if the competition is caused by shape coexistence, why is no such shape coexistence known in the neighboring nuclei? It is possible to generate a competition between a single band and a chiral pair if, for instance, the former corresponds to an axially symmetric shape while the latter corresponds to triaxial deformation. But lifetime measurements were carried out for the three $\pi h_{9/2} \otimes \nu i_{13/2}{}^{-3}$ bands in ^{194}Tl, and no evidence for differences in the nuclear shape were found.

In the present work the ^{193}Tl nucleus was investigated in order to search for chiral structures and in particular to find out whether similar band competition exists. The present work reports on the negative parity part of the level scheme, focusing on the rotational bands with $\pi h_{9/2} \otimes \nu i_{13/2}{}^{-2}$ nature. Preliminary results were published in [68–71]. The present paper supersedes these publications.

II. EXPERIMENTS AND DATA ANALYSIS

Two experiments were performed at iThemba LABS in South Africa. Accelerated particle beams were delivered by the Separated Sector Cyclotron (SSC). The γ rays de-exciting the high-spin states in ^{193}Tl were registered with the AFRODITE array comprising nine Compton-suppressed clover detectors, five of which were placed at $\theta = 90^\circ$ and four at $\theta = 135^\circ$ with respect to the beam direction. The ^{193}Tl nuclei were produced using two heavy-ion fusion-evaporation reactions: ^{160}Gd(^{37}Cl, $4n$) at a beam energy of 167 MeV and ^{181}Ta(^{18}O, $6n$) at a beam energy of 105 MeV. A self-supported target of 1.0 mg/cm^2 was used in both reactions. The trigger condition required at least two γ rays detected in the clover detectors within a coincidence window of 180 ns. Digital electronics [72] were used for the data collection in the second experiment with the ^{181}Ta(^{18}O, $6n$) reaction. It allowed high data-collection rates due to reduced dead time. About 10^{10} γ-γ events were gathered in the second experiment.

Data were sorted into matrices and spectra and analyzed with the RADWARE software package [73]. The level scheme

*Corresponding author: elena@tlabs.ac.za

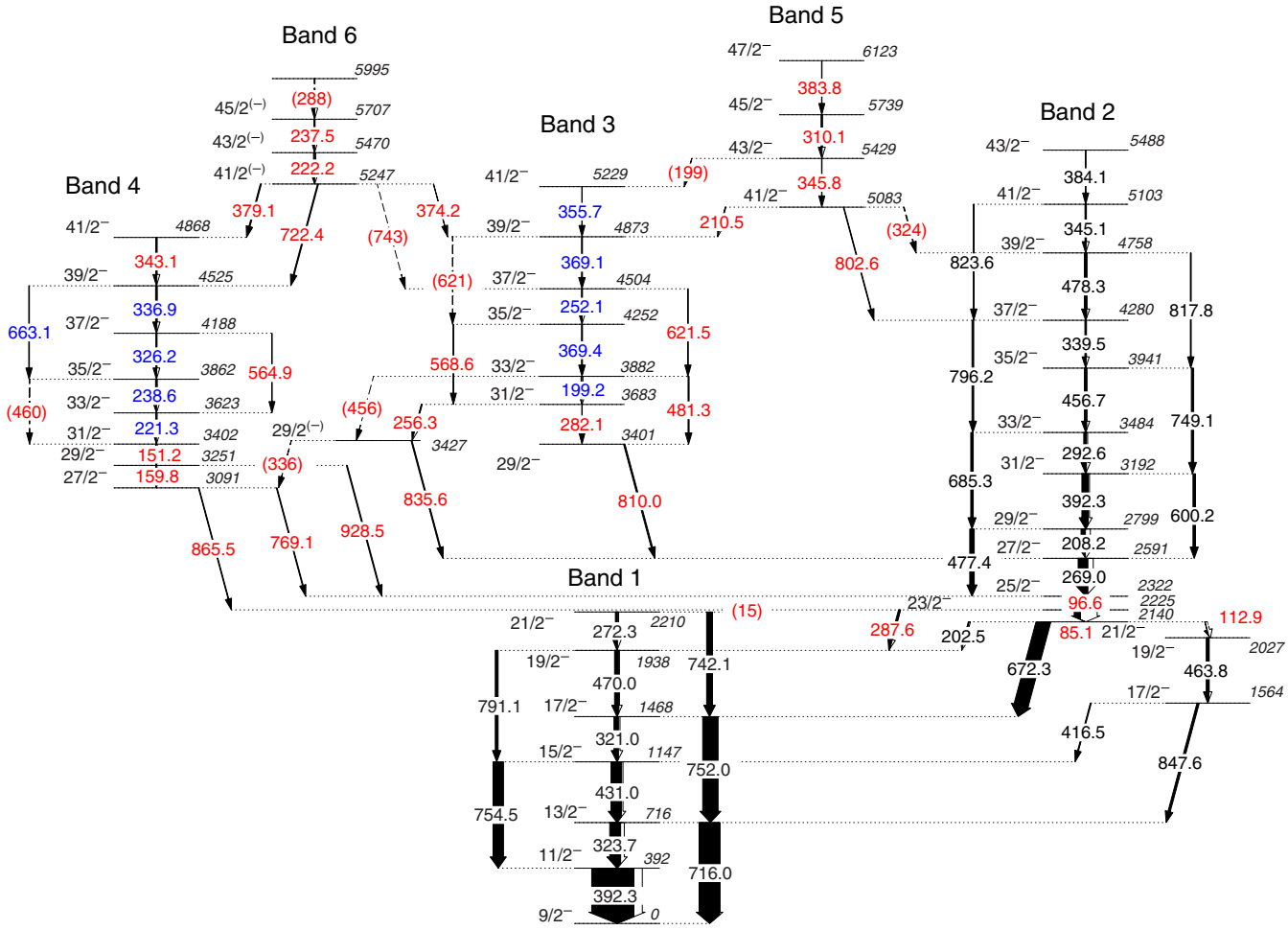

FIG. 1. Partial level scheme of ^{193}Tl. New transitions are shown in red. Transitions with revised placement are shown in blue.

was constructed based on the analysis of the coincidence relationships. Spins were assigned to levels based on angular distribution ratio measurements, applied as described in [24]. Isotropically gated background-subtracted spectra were used to measure the angular distribution ratio:

$$R_{AD}^{\exp} = \frac{I_\gamma(135^\circ)}{I_\gamma(90^\circ)}, \tag{1}$$

where $I_\gamma(135^\circ)$ is the intensity of the γ ray of interest at 135°, and $I_\gamma(90^\circ)$ is the intensity at 90°. The measured $R_{AD}^{\exp}$ ratios are very similar to the theoretical angular distribution ratios of $R_{AD}^{th} = 0.85$ for pure stretched dipole and $R_{AD}^{th} = 1.35$ for pure stretched quadrupole transitions, calculated assuming $\sigma/I = 0.3$ (σ is the Gaussian parameter describing the alignment of the angular momentum I in a plane perpendicular to the beam axis [74]). Electric or magnetic nature of strong transitions was determined in linear polarization anisotropy measurements, as described in [24]. The polarization anisotropy is expressed as

$$A_p = \frac{N_V - \varepsilon N_H}{N_V + \varepsilon N_H},$$

where N_V and N_H are the number of double-hit events scattered in the vertical (perpendicular to the beam line) and horizontal (parallel to the beam line) directions respectively, and ε is the relative efficiency of the detector crystals (in this case $\varepsilon = 1.0$). A_p has positive sign for stretched electric transitions and negative sign for stretched magnetic transitions. The γ-ray intensities were measured using isotropically gated spectra.

III. RESULTS

The analysis of the data resulted in an extension and a revision of the previous level scheme [75]. A partial level scheme of ^{193}Tl obtained in this work and depicting the negative-parity bands is shown in Fig. 1. The results from the experimental measurements for different γ-ray transitions from the 6n reaction are shown in Table I.

The analysis of the γ-γ coincidences was complex due to a number of transitions having the same or similar energies. Thus, a spectrum gated on a transition of interest often showed other decay paths too. In many cases the difference of two spectra, gated on transitions with similar, but unequal energies were analyzed to distinguish different decay paths. In some cases, where the statistics of the triple γ-γ-γ events allowed, information could be extracted from double-gated spectra.

TABLE I. List of the energies, γ-ray intensities, angular distribution ratios, linear polarization anisotropy, energy of the initial levels, and corresponding spin and parity assignments for the γ-ray transitions in ^{193}Tl.

E_γ (keV)[a]	I_γ	R_{AD}	A_p	E_i (keV)	$I_i^\pi \rightarrow I_f^\pi$
(15)				2225	$23/2^- \rightarrow 21/2^-$
85.1				2225	$23/2^- \rightarrow 21/2^-$
96.6	5.1(14)	0.87(17)		2322	$25/2^- \rightarrow 23/2^-$
112.9	0.9(2)	0.85(25)		2140	$21/2^- \rightarrow 19/2^-$
151.2	1.0(2)	0.76(19)		3402	$31/2^- \rightarrow 29/2^-$
159.8	0.8(2)	0.74(21)		3251	$29/2^- \rightarrow 27/2^-$
199.2	2.4(5)	0.79(11)		3882	$33/2^- \rightarrow 31/2^-$
202.5	2.2(4)	0.90(14)		2140	$21/2^- \rightarrow 19/2^-$
208.2	10.4(21)	0.82(12)		2799	$29/2^- \rightarrow 27/2^-$
210.5	0.7(3)	0.73(28)		5083	$41/2^- \rightarrow 39/2^-$
221.3	1.8(4)	0.83(8)		3623	$33/2^- \rightarrow 31/2^-$
222.2	2.7(4)			5470	$43/2^{(-)} \rightarrow 41/2^{(-)}$
237.5	3.7(5)[b]	0.77(12)[b]		5707	$45/2^{(-)} \rightarrow 43/2^{(-)}$
238.6	3.7(5)[b]	0.77(12)[b]		3862	$35/2^- \rightarrow 33/2^-$
252.1	1.4(2)	0.85(24)		4504	$37/2^- \rightarrow 35/2^-$
256.3	1.4(4)	0.81(28)		3683	$31/2^- \rightarrow 29/2^{(-)}$
269.0	23.1(24)	0.78(9)	−0.04(4)	2591	$27/2^- \rightarrow 25/2^-$
272.3	5.0(3)	0.81(21)		2210	$21/2^- \rightarrow 19/2^-$
282.1	0.7(2)	0.51(26)		3683	$31/2^- \rightarrow 29/2^-$
287.6	4.3(12)	1.12(8)		2225	$23/2^- \rightarrow 19/2^-$
(288)	1.3(5)			5995	$\rightarrow 45/2^{(-)}$
292.6	6.3(14)	0.81(10)		3484	$33/2^- \rightarrow 31/2^-$
310.1	2.5(7)	0.71(21)		5739	$45/2^- \rightarrow 43/2^-$
321.0	10.6(8)	0.85(12)	−0.07(4)	1468	$17/2^- \rightarrow 15/2^-$
323.7	25.9(58)	0.86(9)	−0.13(5)	716	$13/2^- \rightarrow 11/2^-$
(324)				5083	$41/2^- \rightarrow 39/2^-$
326.2	2.0(6)	0.74(9)		4188	$37/2^- \rightarrow 35/2^-$
(336)				3427	$29/2^{(-)} \rightarrow 27/2^-$
336.9	3.0(6)	0.68(19)		4525	$39/2^- \rightarrow 37/2^-$
339.5	2.9(5)	0.74(10)		4280	$37/2^- \rightarrow 35/2^-$
343.1	2.5(7)	0.65(29)		4868	$41/2^- \rightarrow 39/2^-$
345.1	2.6(6)	0.76(25)	−0.09(9)	5103	$41/2^- \rightarrow 39/2^-$
345.8	0.8(2)	0.87(21)		5429	$43/2^- \rightarrow 41/2^-$
355.7	0.8(3)	0.77(23)		5229	$41/2^- \rightarrow 39/2^-$
369.4	3.7(7)[b]	0.70(12)[b]		4252	$35/2^- \rightarrow 33/2^-$
369.1	3.7(7)[b]	0.70(12)[b]		4873	$39/2^- \rightarrow 37/2^-$
374.2	0.7(3)	0.69(20)		5247	$41/2^{(-)} \rightarrow 39/2^-$
379.1	2.1(5)			5247	$41/2^{(-)} \rightarrow 41/2^-$
383.8	1.8(2)[b]	0.85(29)[b]		6123	$47/2^- \rightarrow 45/2^-$
384.1	1.8(2)[b]	0.85(29)[b]		5488	$43/2^- \rightarrow 41/2^-$
392.3	100.0(5)	0.91(8)	−0.02(3)	392	$11/2^- \rightarrow 9/2^-$
392.3	15.1(20)	0.78(12)		3192	$31/2^- \rightarrow 29/2^-$
416.5	2.0(5)			1564	$17/2^- \rightarrow 15/2^-$
431.0	24.5(25)	0.79(8)	−0.04(3)	1147	$15/2^- \rightarrow 13/2^-$
(456)				3882	$33/2^- \rightarrow 29/2^{(-)}$
456.7	5.4(13)	0.65(28)	−0.03(4)	3941	$35/2^- \rightarrow 33/2^-$
(460)	1.0(2)			3862	$35/2^- \rightarrow 31/2^-$
463.8	6.3(8)	0.73(17)		2027	$19/2^- \rightarrow 17/2^-$
470.0	10.3(11)	0.82(17)		1938	$19/2^- \rightarrow 17/2^-$
477.4	10.3(14)	1.28(28)		2799	$29/2^- \rightarrow 25/2^-$
478.3	5.6(11)	0.83(8)		4758	$39/2^- \rightarrow 37/2^-$
481.3	2.4(3)	1.19(17)		3882	$33/2^- \rightarrow 29/2^-$
564.9	0.7(2)	1.15(11)		4188	$37/2^- \rightarrow 33/2^-$
568.6	0.9(4)			4252	$35/2^- \rightarrow 31/2^-$

TABLE I. (*Continued.*)

E_γ (keV)[a]	I_γ	R_{AD}	A_p	E_i (keV)	$I_i^\pi \rightarrow I_f^\pi$
600.2	5.8(16)			3192	$31/2^- \rightarrow 27/2^-$
(621)				4873	$39/2^- \rightarrow 35/2^-$
621.5	2.4(4)	1.41(11)		4504	$37/2^- \rightarrow 33/2^-$
663.1	1.5(6)	1.31(20)		4525	$39/2^- \rightarrow 35/2^-$
672.3	33.6(35)	1.21(15)	0.04(3)	2140	$21/2^- \rightarrow 17/2^-$
685.3	5.8(21)	1.25(11)	0.07(5)	3484	$33/2^- \rightarrow 29/2^-$
716.0	49.0(55)	1.29(23)	0.06(3)	716	$13/2^- \rightarrow 9/2^-$
722.4	2.3(5)			5247	$41/2^{(-)} \rightarrow 39/2^-$
742.1	13.8(15)	1.29(25)		2210	$21/2^- \rightarrow 17/2^-$
(743)	0.4(1)			5247	$41/2^{(-)} \rightarrow 37/2^-$
749.1	5.4(13)	1.21(14)		3941	$35/2^- \rightarrow 31/2^-$
752.0	36.0(54)	1.20(34)		1468	$17/2^- \rightarrow 13/2^-$
754.5	24.5(53)	1.25(12)		1147	$15/2^- \rightarrow 11/2^-$
769.1	1.8(6)	0.76(37)	−0.05(5)	3091	$27/2^- \rightarrow 25/2^-$
791.1	6.6(12)	1.13(11)	0.04(3)	1938	$19/2^- \rightarrow 15/2^-$
796.2	4.0(7)	1.15(8)	0.08(5)	4280	$37/2^- \rightarrow 33/2^-$
802.6	1.5(4)			5083	$41/2^- \rightarrow 37/2^-$
810.0	3.2(9)	0.53(13)	−0.04(5)	3401	$29/2^- \rightarrow 27/2^-$
817.8	2.0(5)	1.30(11)		4758	$39/2^- \rightarrow 35/2^-$
823.6	2.0(6)	1.32(20)		5103	$41/2^- \rightarrow 37/2^-$
835.6	2.4(4)			3427	$29/2^{(-)} \rightarrow 27/2^-$
847.6	5.3(8)	1.13(21)		1564	$17/2^- \rightarrow 13/2^-$
865.5	1.7(5)	1.16(25)		3091	$27/2^- \rightarrow 23/2^-$
928.5	2.1(4)	1.17(31)		3251	$29/2^- \rightarrow 25/2^-$

[a]Typical uncertainty is 0.3 keV and up to 0.5 keV for doublets and weak transitions.
[b]Doublet transition; the intensity is measured for the total peak.

Band 2 is the most intense negative-parity band; it was reported in a previous study [75]. In this work two new low-energy transitions were discovered and placed in the band-crossing region of Bands 1 and 2. This led to a change of the spins of the levels in Band 2; they were increased by $2\hbar$. The 96.6-keV transition is a new transition, different from the transition with similar energy, previously placed in coincidence with the positive-parity states in ^{193}Tl [75]. Furthermore it is in coincidence with the γ rays emitted from the negative-parity states, as illustrated in the spectra in Figs. 2 and 3. The new 85.1-keV γ-ray peak overlaps with the K_β x-rays of Tl. Evidence for the presence of this γ ray is shown in the insets of Fig. 2, where a strong enhancement at 85.1 keV is observed in the spectrum gated on 672.3 keV in comparison with the corresponding peak in the spectrum gated on the 287.6-keV transition, (the latter transition is in anticoincidence with the 85.1-keV γ ray).

Band 3 is a weaker band. Some of its transitions were observed previously [75]. This earlier work, however, suggested tentative spins for its levels and could not assign parity. In the present work Band 3 was extended, revised, and in addition spin and parity were assigned. Band 3 was connected to Band 2 in a different way, through new linking transitions with energies of 810.0 and 835.6 keV. The linking transitions can be identified in the gated spectra shown in Fig. 2.

As an example of the γ-coincidence analysis, the placement of the 369-keV transitions is discussed. Three transitions with similar energies of 369.4, 369.1, and 368 keV were found to belong to ^{193}Tl. The analysis showed that the 368-keV γ ray belongs to the positive-parity part of the level scheme. The spectrum shown in Fig. 2(c) is gated on the 369-keV peak. The presence of a peak at 369.4 keV confirms that two of the 369-keV transitions are in coincidence with each other. This spectrum also shows a number of transitions from the negative-parity states of ^{193}Tl, denoted with their energies, but also many γ rays associated with decays from the positive-parity states, denoted with stars ($*$). To establish the placement of the two coincident 369-keV transitions, a spectrum that is the difference between spectra gated on the 369- and 368-keV transitions (using a suitable normalization factor) was examined; see Fig. 2(b). It shows a substantially decreased, almost completely missing contribution from the γ rays belonging to the positive-parity structures in ^{193}Tl. It also shows a peak at 369.4 keV, as well as the transitions from Band 3. It illustrates that the two 369-keV γ rays belong to the negative-parity part of the level scheme. A spectrum double gated on the 369-keV transitions is plotted in Fig. 2(a). It shows transitions from the negative-parity bands of ^{193}Tl, confirming that both 369-keV transitions feed the negative-parity states and also transitions from Band 3. In a previous work one of the 369-keV transitions was placed in Band 3, while the second one was suggested as a linking transition between Band 3 and Band 2, [75]. It was placed in anticoincidence with the 256.3-keV transition. The spectrum double-gated on 369 keV, however, shows that both 369-keV transitions are in coincidence with the 256.3-keV γ ray, and also with the 810.0- and 835.6-keV linking transitions. Both 369-keV transitions are therefore in-band transitions.

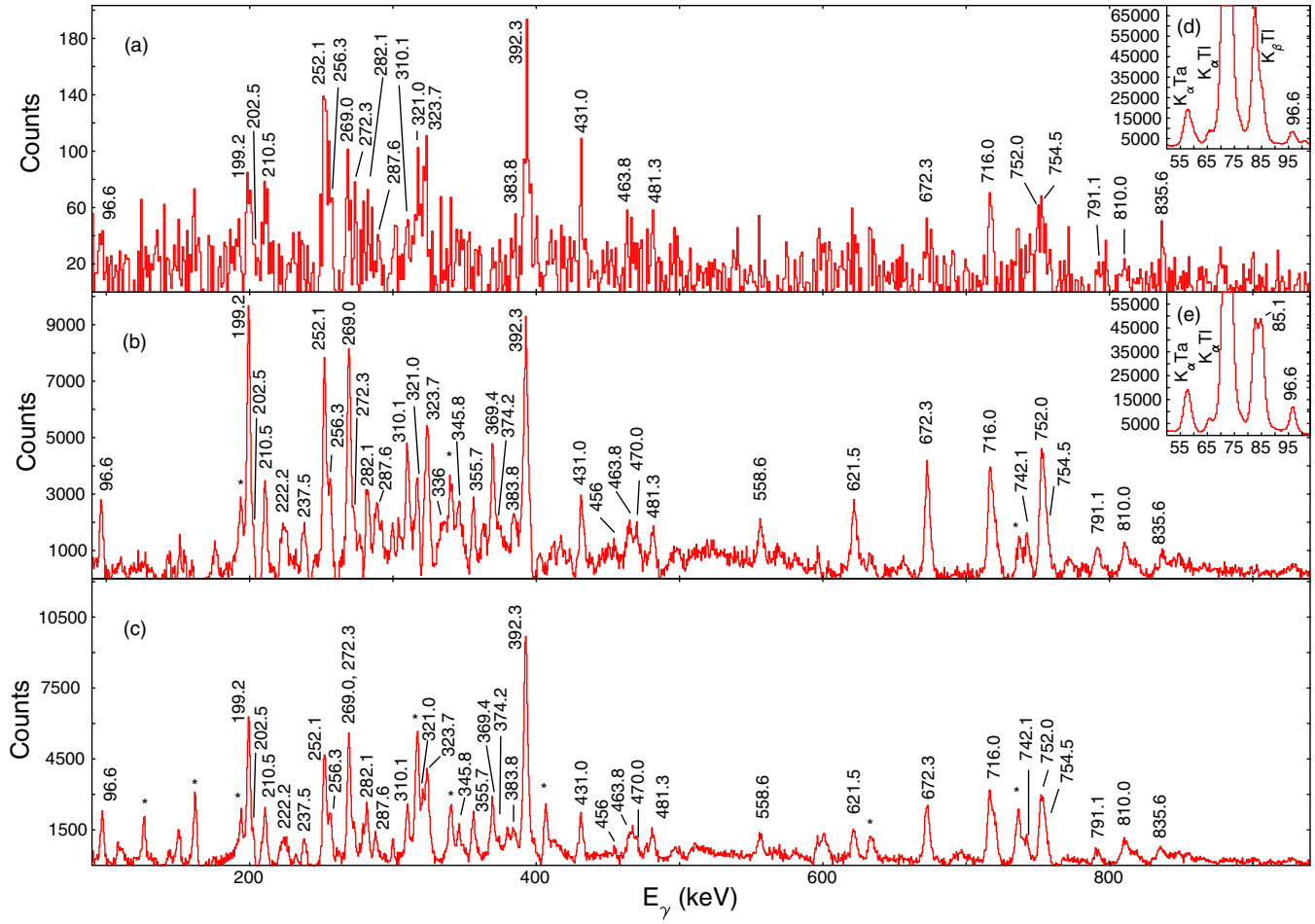

FIG. 2. Illustration of the transitions placed in Bands 3, 5, and 6, and also the new 85.1- and 96.6-keV γ rays of Band 2. (a) Spectrum, double-gated on the 369-keV peak. (b) A spectrum made as a difference of two spectra single-gated on the 369- and 368-keV peaks. (c) A spectrum single-gated on the 369-keV peak. Insets (d) and (e) show the low-energy part of the spectra gated on the 287.6- and the 672.3-keV peaks, respectively, illustrating the placement of the 85.1-keV transition in anticoincidence with the former transition. Transitions marked with stars ($\star$) belong to the positive-parity part of the level scheme.

The spin assignments of Band 3 are based on the angular distribution ratio of the 810.0-keV linking transition. This transition was assigned a stretched dipole nature (see Table I), suggesting $I = 29/2$ for the 3401-keV level. Band 3 looks very similar to the negative-parity Band 1A in ^{194}Tl. The linear polarization anisotropy A_p was measured for the 810-keV linking transition; it is consistent with a magnetic nature, but the uncertainty is large. However the angular distribution ratio R_{AD} shows a very strong asymmetry, which is only compatible with a mixed transition, thus the 810-keV transition was assigned a mixed $M1 + E2$ multipolarity.

Some of the transitions of Band 4 were observed previously, but they were placed in a sequence feeding the positive-parity levels in ^{193}Tl [75]. In the present work this band was extended, placed differently by linking it to the negative-parity states, and assigned spin and parity. As an illustration of a complex analysis for this band, the placement of the 221.3-keV transition is discussed below. Another transition with similar energy of 220.5 keV belongs to the positive-parity structures. Thus, a spectrum single-gated on the 221-keV peak [see Fig. 3(c)] shows transitions from both the positive-parity structures (marked with stars in the figure), and from the negative-parity bands (marked with their energies). However, a spectrum made as a difference between the spectra gated on 221 and on 220 keV transition [see Fig. 3(b)] illustrates an enhancement of the γ rays that belong to the negative-parity structures, while the peaks from the positive-parity γ rays decrease in intensity. An enhancement of the transitions of Band 4 is also noticeable; compare for instance the intensity of the 238-kev peak with respect to the 392.3-keV peak. This suggests that the 221.3-keV γ ray is in coincidence with the negative-parity structures in ^{193}Tl.

Band 4 was extended with four new transitions (see Fig. 1), and linked towards the band-crossing region of Bands 1 and 2 with three new transitions with energies of 928.5, 865.5, 769.1 keV. The spin assignments for this band were determined based on the angular distribution ratios for the three linking transitions. They were assigned stretched quadrupole, stretched quadrupole and stretched dipole nature, respectively (see Table I), which suggests $I = 27/2$ for the 3091-keV level.

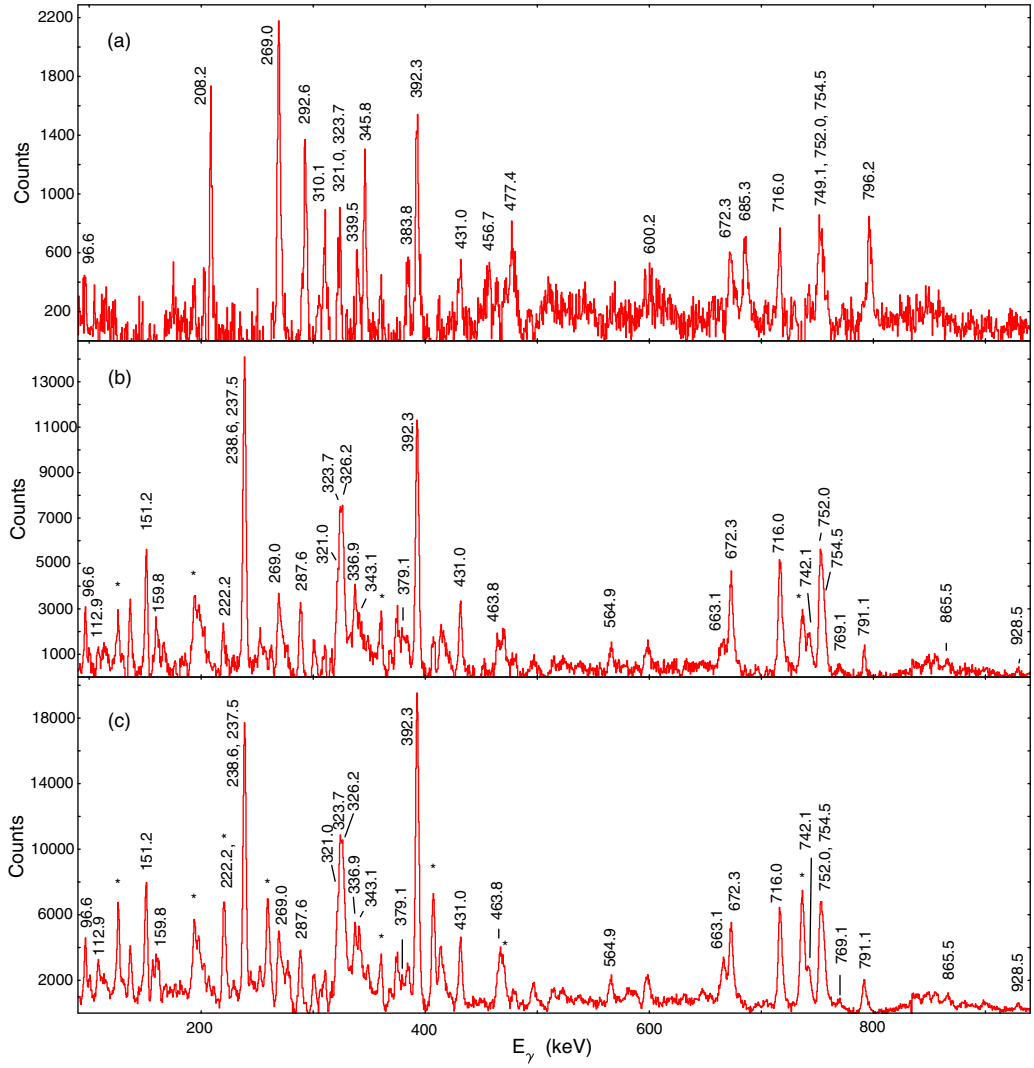

FIG. 3. Illustration of the transitions placed in Bands 4 and 5. (a) Spectrum gated on the 802.6-keV transition. (b) A spectrum made as a difference between the spectra gated on the 221.3- and the 220.5-keV transitions. (c) Spectrum gated on the 221.3-keV peak. Transitions marked with stars (⋆) belong to the positive-parity part of the level scheme.

This band is similar to the negative-parity Band 4A in ^{194}Tl. Linear polarization measurements for the three linking transitions yielded results with large uncertainties. Nevertheless Band 4 was assigned negative parity, because the alternative positive parity assignment would require that the stretched quadrupole transitions have $M2$ nature.

The coincidence analysis revealed two new bands, Bands 5 and 6, lying at higher excitation energy. Linking transitions from Band 5 to Bands 2 and 3 were identified. Based on the measured stretched dipole character of the 210.5-keV transition, $I = 41/2$ was assigned to the 5083-keV bandhead level. The presence of the 802.6-keV stretched quadrupole transition indicates that this level (and probably all of Band 5) have negative parity. Spectra gated on the 369-keV transition(s) (see Fig. 2) and the spectrum gated on the 802.6-keV transition [see Fig. 3(a)] illustrate the γ rays placed in Bands 5.

Band 6 (see Fig. 1), decays towards Bands 3 and 4 through the 379.1- and 374.2-keV linking transitions. The stretched dipole nature of the 374.2-keV γ ray suggests $I = 41/2$ for the bandhead level. Tentative negative parity was assigned to this band. The γ rays placed in Band 6 are illustrated in the spectra gated on 369 keV (see Fig. 2) and on 221.3 keV [see Figs. 3(b) and 3(c)].

IV. DISCUSSION

The proton and neutron Fermi levels in the Tl isotopes in the 190 mass region lie near the bottom of the $\pi h_{9/2}$ shell and near the top of the $\nu i_{13/2}$ shell, respectively. The $h_{9/2}$ proton angular momentum aligns along the short nuclear axis, while the $i_{13/2}$ neutron angular momenta align along the long nuclear axis. Chiral systems with $\pi h_{9/2} \otimes \nu i_{13/2}^{-n}$ nature were previously reported in ^{194,195,198}Tl [17,18,23–25,53]. The ^{194,195}Tl nuclei were studied up to high spins where three- and four-quasiparticle bands form. The published results on ^{195}Tl are still partial; they show a $\pi h_{9/2} \otimes \nu i_{13/2}^{-2}$ chiral pair but do not mention a competing band with the same

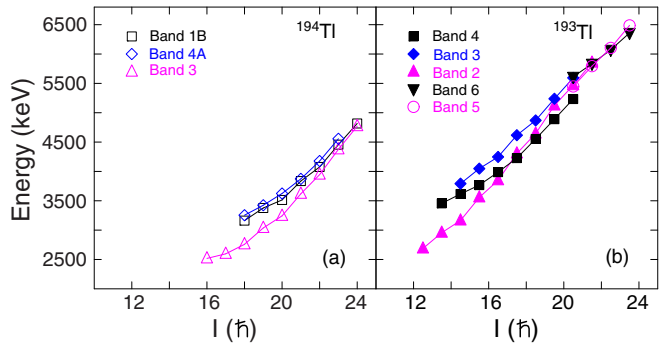

FIG. 4. Excitation energies for the $\pi h_{9/2} \otimes \nu i_{13/2}^{-n}$, where $n = 2, 3, 4$ bands in ^{194}Tl (a) and in ^{193}Tl (b).

configuration. Therefore we will illustrate the open questions arising from the observation of multiple $\pi h_{9/2} \otimes \nu i_{13/2}^{-n}$ bands using experimental data on ^{194}Tl.

Three rotational bands with $\pi h_{9/2} \otimes \nu i_{13/2}^{-3}$ nature were observed in ^{194}Tl [24]; their excitation energies and alignments are shown in Figs. 4 and 5. The additivity rule works very well for the alignments in this mass region. For instance the alignment measured in a rotational band in a Tl isotope matches very well the sum of (i) the alignment of the odd $h_{9/2}$ proton calculated from the experimental data for a $9/2^-$

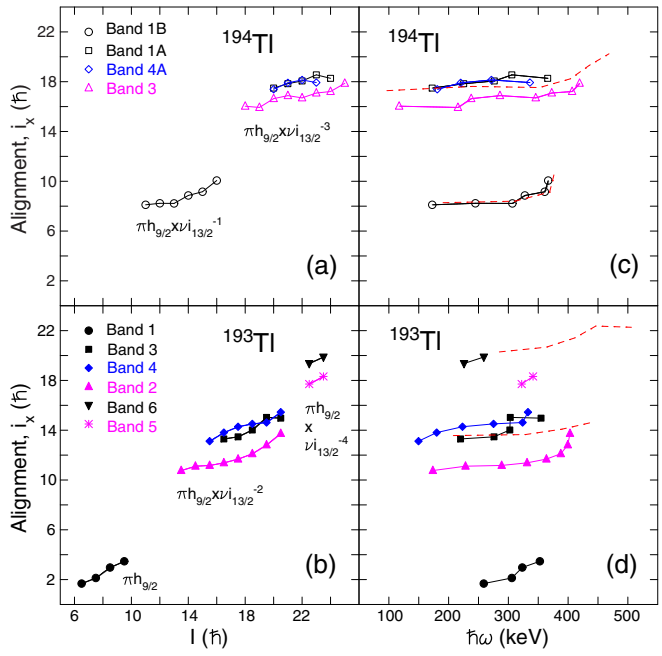

FIG. 5. Alignments for the $\pi h_{9/2} \otimes \nu i_{13/2}^{-n}$ bands, where $n = 0, 1, 2, 3, 4$ in ^{193,194}Tl as a function of the initial spin I in panels (a) and (b), and as a function of the rotational frequency in panels (c) and (d). Harris parameters of $J_0 = 8\hbar^2/\text{MeV}$ and $J_1 = 40\hbar^4/\text{MeV}^3$ [24,77] were used. The red dashed line in panels (c) and (d) indicates the experimental alignment of the corresponding $\nu i_{13/2}{}^{-n}$ band in the Hg isotone (data taken from [77]) increased by $2.1\hbar$, a value that corresponds to the approximate alignment of the $h_{9/2}$ proton.

band in an odd-Tl isotope, and (ii) the alignment of the $i_{13/2}$ neutrons, calculated from the corresponding yrast band in the Hg isotone. There is an excellent agreement between the measured alignment of the yrast 8^- band with $\pi h_{9/2} \otimes \nu i_{13/2}^{-1}$ configuration in ^{194}Tl (labeled Band 1B in Figs. 5(c) and 5(d), as in [24]) and the sum of the alignments of the $9/2^-$ band with $\pi h_{9/2}$ configuration in ^{193}Tl and the $13/2^+$ band with $\nu i_{13/2}^{-1}$ configuration in ^{193}Hg; the sum is shown with a red dashed line in Fig. 5(c). Excellent agreement is also obtained for the positive-parity bands in ^{194}Tl, built on the $\pi h_{9/2} \otimes \nu i_{13/2}^{-1} \nu j$ configuration (where j is a low-spin neutron from the $p_{3/2}$, $p_{1/2}$, and $f_{5/2}$ shells; see Fig. 8 in [24]), and also for the chiral pair bands, built on the $\pi h_{9/2} \otimes \nu i_{13/2}^{-3}$ configuration, shown in Fig. 5(c). However, the third $\pi h_{9/2} \otimes \nu i_{13/2}^{-3}$ band, labeled Band 3 in Figs. 5(a) and 5(c), has about $1.5-2\,\hbar$ lower alignment than expected. The nature of this third $\pi h_{9/2} \otimes \nu i_{13/2}^{-3}$ band looks very curious as it is not easy to understand its lower alignment.

In previous works a few possible interpretations for this band were considered. It was thought, for instance, that the chiral pair and the third band might correspond to different nuclear shapes [24], e.g., triaxial and axially symmetric, respectively. Subsequently lifetime measurements were carried out [25]. The results showed that all three bands have very similar $B(M1)$ and $B(E2)$ reduced transition probabilities, with no evidence of any differences in the nuclear shape or configuration. In addition many-particle rotor (MPR) model calculations were performed [25]. They assumed a shape with a triaxial deformation of $\gamma = -40°$, as suggested by the cranked Nilsson-Strutinsky (CNS) potential energy surface minimum [23]. The MPR calculations indicated that several bands of $\pi h_{9/2} \otimes \nu i_{13/2}^{-3}$ nature form at similar excitation energy. All of these bands correspond to chiral geometry of the angular momenta. Most interesting, however, is that the calculated bands do not pair into easily distinguishable (by their excitation energy) partner bands. Instead they split into an yrast $\pi h_{9/2} \otimes \nu i_{13/2}^{-3}$ band and three other $\pi h_{9/2} \otimes \nu i_{13/2}^{-3}$ bands lying at higher (and similar) energy, see Fig. 4 of [25]. Further theoretical calculations suggested that this behavior is not unusual. In fact the partner bands of a multiple chiral system often do not group in obvious pairs [76]. Difficulties with grouping rotational bands into chiral pairs were also reported for the experimental data in ^{103}Rh [64]. Therefore another possible interpretation was considered for the bands in ^{194}Tl. It was argued that the three $\pi h_{9/2} \otimes \nu i_{13/2}^{-3}$ bands may indicate the formation of two chiral systems, in which the partner bands have split, producing one yrast band and three higher-energy bands, of which the fourth partner is still missing [25]. This suggestion looked very promising, although it relied on the assumption that there exists a fourth partner band.

In order to further investigate the nature of the negative-parity bands in the Tl isotopes, we studied ^{193}Tl to understand the systematic behavior of the competing $\pi h_{9/2} \otimes \nu i_{13/2}^{-n}$ bands. Most interesting was to test the idea of the formation of two chiral systems.

Three negative-parity bands, Bands 2, 3, and 4, were observed in ^{193}Tl and assigned $\pi h_{9/2} \otimes \nu i_{13/2}^{-2}$ configuration.

Bands 3 and 4 have similar alignment of about 14$\hbar$ [see Fig. 5(b)], while Band 2 has an alignment of about 12 $\hbar$. The three negative-parity bands look very similar to their counterparts in ^{194}Tl; see Fig. 5(a). The alignment of Bands 3 and 4 matches well the expected alignment for a $\pi h_{9/2} \otimes \nu i_{13/2}^{-2}$ band if one applies the sum rule using the measured alignments of the $h_{9/2}$ proton and the two $i_{13/2}$ neutrons; see the dashed red line in Fig. 5(d). As in ^{194}Tl, Band 2 has an alignment that is lower than expected (by 2−2.5 $\hbar$). As in ^{194}Tl, a fourth band with the same configuration could not be observed.

The three $\pi h_{9/2} \otimes \nu i_{13/2}^{-2}$ bands in ^{193}Tl lie at similar excitation energy, as in ^{194}Tl, but they show a new feature: there is a crossing between Bands 2 and 4; see Fig. 4. This is a crossing between two bands with the same parity, therefore one would expect them to interact with each other. However, there is no evidence for considerable interaction, thus it seems that there should be an important difference in the nature of the bands.

Another new feature of the three bands in ^{193}Tl is that they were extended through another neutron $i_{13/2}$ pair alignment, into Bands 5 and 6. Note that the ≈2$\hbar$ difference in the alignment persists for the five-quasiparticle bands. For instance, the expected alignment for the $\pi h_{9/2} \otimes \nu i_{13/2}^{-4}$ configuration, shown with a red dashed line in Fig. 5(d), matches well the alignment of Band 6. However Band 5, which is an extension of Band 2, has lower than expected alignment. This suggests that the difference in the nature of these $\pi h_{9/2} \otimes \nu i_{13/2}^{-n}$ bands persists for the five-quasiparticle configuration too.

The idea that these negative-parity bands may reflect the presence of two chiral systems requires the observation of four bands with the same nature. However, as in ^{194}Tl, a fourth band was not observed in ^{193}Tl. This suggests that the experimental data show no evidence for a possible second chiral system built on the same configurations. To understand these bands better we investigated the alignment properties of the valence neutrons in the neighboring nuclei.

It is known that the Au isotopes in this mass region show an interesting alignment behavior: rotational bands with incomplete neutron alignment [78]. For instance the $\pi h_{11/2} \otimes \nu i_{13/2}^{-n}$ bands with $n = 1, 2$ involve $\pi h_{11/2}$ and $\nu i_{13/2}$ orbitals from the top of the corresponding shells. Such valence particles align their angular momenta along the same (long) nuclear axis. For axially symmetric shape, decoupled bands with full alignment of the particle angular momenta are expected. However, isomeric states with lower spin are observed. For instance the yrast $\pi h_{11/2} \otimes \nu i_{13/2}^{-1}$ configuration in the odd-odd ^{188,190,192,194}Au nuclei produces the $I^{\pi} = 11^{-}$ isomeric state, instead of the fully aligned $I^{\pi} = 12^{-}$ state. Moreover the $\pi h_{11/2} \otimes \nu i_{13/2}^{-2}$ configuration produces the partially aligned $I^{\pi} = 31/2^{-}$ isomer in ^{189,191}Au while the fully aligned state would have $I^{\pi} = 35/2^{-}$ (evaluated experimental data on these Au isotopes can be found in [79–84]).

The lowering in energy of the partially aligned states in the Au isotopes was explained as being caused by the nonaxial shape of the nucleus and in particular by its rotation around the long nuclear axis, with $\gamma \approx -70^{\circ}$ to $\approx -90^{\circ}$ [78]. It was shown that for $\gamma < -80^{\circ}$ the energy of the Routhians originating from the neutron $i_{13/2}$ configurations changes considerably; for instance, for $\gamma \approx -90^{\circ}$ the Routhian with largest alignment, A, moves up to higher energy, and lies well above the lower-alignment B and C Routhians; see Fig. 8 in [78]. This explains the ≈2$\hbar$ lower than expected spin of the yrast $\pi h_{11/2} \otimes \nu i_{13/2}^{-2}$ states in the ^{189,191,193}Au isotopes. We suggest that a similar phenomenon plays a role in the rotational bands of the Tl isotopes.

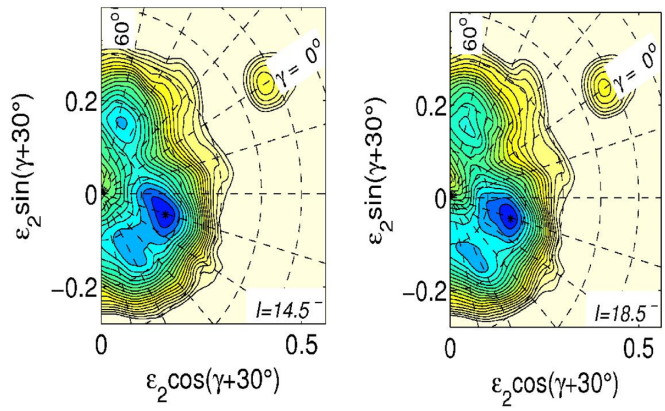

FIG. 6. Potential energy surfaces calculated with the cranked Nilsson-Strutinsky codes for the $\pi h_{9/2} \otimes \nu i_{13/2}^{-2}$ bands in ^{193}Tl.

Cranked-Nilsson-Strutinsky calculations with standard parameters for the Nilsson potential [85,86] were carried out for ^{193}Tl. The potential energy surfaces for the $\pi h_{9/2} \otimes \nu i_{13/2}^{-2}$ bands are shown in Fig. 6. The absolute minimum in the potential energy surfaces corresponds to a triaxial shape with $\varepsilon_2 = 0.15$ and a nonaxiality parameter $\gamma \approx -45^{\circ}$. This minimum suggests that the nucleus rotates around its intermediate axis. Taking into account that the $\pi h_{9/2} \otimes \nu i_{13/2}^{-2}$ configuration involves a proton particle and neutron holes, this minimum supports the formation of a chiral symmetry system. The plot in Fig. 6, however, indicates a secondary minimum at $\gamma \approx -90^{\circ}$. This minimum also corresponds to triaxial shape, but in this case the nucleus rotates around its long axis.

Cranked shell model calculations were carried out for ^{193}Tl. A Nilsson potential with l dependent parameters, as suggested for the neighboring Hg isotopes [87], was used. The neutron Fermi level was set at 50.8 MeV and the pairing gap energy at 1 MeV. The calculations were carried out for quadrupole deformation of $\varepsilon_2 = 0.15$, as suggested by the CNS calculations; see Fig. 6. Several different values of the triaxiality parameter γ were used. The calculated quasineutron Routhians with positive parity are shown in Fig. 7. The four lowest-energy Routhians at $\gamma = -60^{\circ}$ are labeled as A, B, C, and D. They originate from neutron orbitals with $i_{13/2}$ nature, and at $\gamma = -60^{\circ}$ have alignments, as shown in Table II. For $\gamma < -60^{\circ}$ these Routhians are labeled according to their alignments, that is the Routhian with alignment of ≈6.2 is labeled A. The calculations confirm the previous results that the Routhian with largest alignment, A, lies at lowest energy for axially symmetric shape with $\gamma = -60^{\circ}$, but for $\gamma < -60^{\circ}$ this Routhian moves toward higher energies, and for $\gamma = -90^{\circ}$ the lower-alignment Routhians B and C lie below it. Therefore the $\pi h_{9/2} \otimes \nu i_{13/2}^{-2}$ band associated

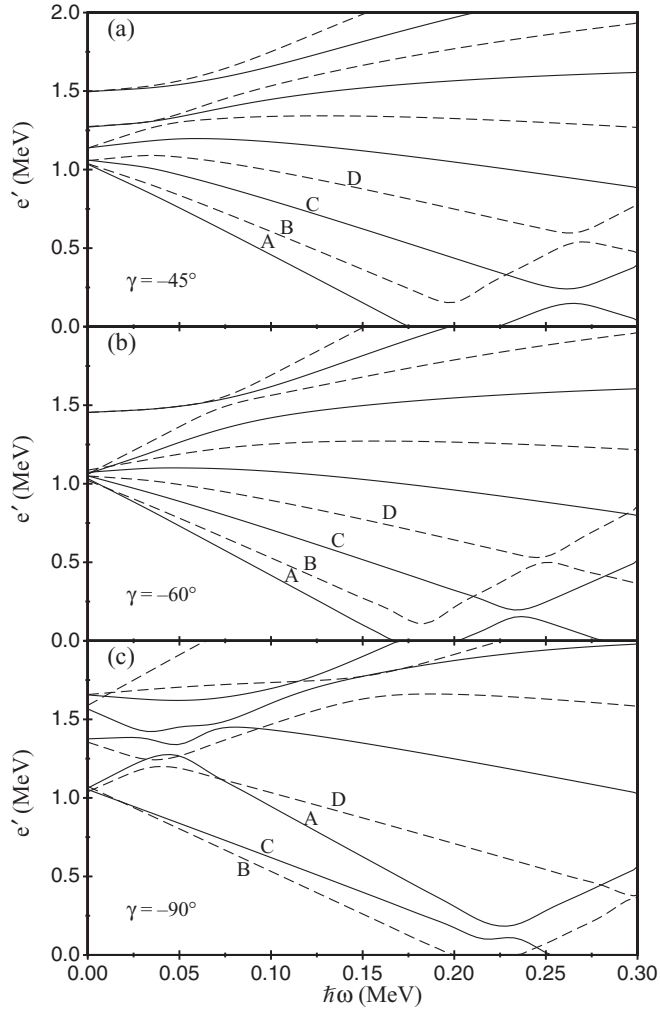

FIG. 7. Positive-parity quasineutron Routhians for ^{193}Tl, calculated with $\varepsilon_2 = 0.15$ and (a) $\gamma = -45^\circ$, (b) $\gamma = -60^\circ$, and (c) $\gamma = -90^\circ$. Routhians with positive signature are shown with solid lines, while those with negative signature are shown with dashed lines.

with this secondary potential minimum would have a lower alignment as it involves *BC* neutron configuration.

Note that for $\gamma > -60^\circ$, where the nucleus rotates around the intermediate axis, there is no change in the relative position of the neutron Routhians. For instance the relative positions and alignments of the neutron *A*, *B*, *C*, and *D* Routhians at $\gamma = -45^\circ$ are very similar to those for $\gamma = -60^\circ$ (see Fig. 7), and suggest that the highest-alignment Routhians *A* and *B* lie at lowest energy. Therefore the $\pi h_{9/2} \otimes \nu i_{13/2}^{-2}$ band associated with the absolute potential energy minimum at $\gamma = -45^\circ$ corresponds to full neutron alignment. Note that for $\gamma = -45^\circ$ the nucleus rotates around its intermediate axis, producing a chiral system.

TABLE II. Cranked shell model Routhians and alignments (calculated at $\hbar\omega = 0.15$ MeV and $\gamma = -60^\circ$) for the positive parity $i_{13/2}$ neutrons in ^{193}Tl.

Label	(π, α)	Alignment ($\hbar$)
A	(+,+)	6.2
B	(+,−)	5.2
C	(+,+)	3.9

Therefore a new interpretation of the negative-parity bands in the Tl isotopes is proposed. It is suggested that the bands with lower alignment, e.g., Band 2 in ^{193}Tl, corresponds to rotation around the long nuclear axis, which causes its lower alignment, while the bands with full alignments, e.g., Bands 3 and 4, are chiral partner bands formed by rotation around the intermediate nuclear axis. Within this scenario several observations can be understood, such as (i) the presence of a three-quasiparticle $\pi h_{9/2} \otimes \nu i_{13/2}^{-2}$ chiral pair, i.e., Bands 3 and 4; (ii) the presence of a third three-quasiparticle $\pi h_{9/2} \otimes \nu i_{13/2}^{-2}$ band at similar energy, which does not form a chiral system and shows no chiral partner; and (iii) the third band has a lower alignment than expected for its configuration. As the bands correspond to rotation around different axes, it is not very likely that they would interact with each other.

V. SUMMARY

In summary, γ-spectroscopy studies were performed for ^{193}Tl resulting in a revision and an extension of the previous level scheme. Three negative parity $\pi h_{9/2} \otimes \nu {i_{13/2}}^{-2}$ bands were observed. The bands were extended to high spins, where another $i_{13/2}$ pair breaks. The three $\pi h_{9/2} \otimes \nu {i_{13/2}}^{-2}$ bands have similar properties; however, two of them have alignments of $\approx 14\hbar$, while the third one, which is the yrast band, has a lower alignment of $\approx 12\hbar$. It is suggested that this is due to a competition between two different modes of rotation: (i) rotation around the intermediate axis, generating a pair of chiral partner bands with large alignment, and (ii) rotation around the long nuclear axis, generating a band with lower alignment. Cranked Nilsson-Strutinsky calculations support this interpretation, showing two competing minima in the potential energy surfaces: (i) a deeper minimum at $\gamma = -45^\circ$, suggesting a rotation around the intermediate axis, and (ii) a secondary minimum at $\gamma \approx -90^\circ$, associated with a rotation around the long nuclear axis. Cranked shell model calculations explain the difference in the alignments of these bands. They show that for large negative γ deformations, e.g., for $\gamma \approx -90^\circ$, the Routhian with neutron $i_{13/2}$ nature and largest alignment, *A*, moves upwards in energy, and above the *B* and *C* Routhians with the same nature but lower alignments. Thus, the corresponding $\pi h_{9/2} \otimes \nu {i_{13/2}}^{-2}$ band has lower alignment, as its configuration involves a *BC* neutron configuration. Further studies in the neighboring Tl isotopes can shed more light on this very interesting competition.

ACKNOWLEDGMENTS

We are thankful to the crew of the iThemba LABS separated sector cyclotron for the beam delivery. This work is based upon research supported by the National Research Foundation, South Africa under grants with GUN: 93531, 109134, 116666, and 90741.

[1] S. Frauendorf and J. Meng, Nucl. Phys. A **617**, 131 (2006).
[2] D. L. Balabanski, M. Danchev, D. J. Hartley, L. L. Riedinger, O. Zeidan, J. Y. Zhang, C. J. Barton, C. W. Beausang, M. A. Caprio *et al.*, Phys. Rev. C **70**, 044305 (2004).
[3] R. A. Bark, A. M. Baxter, A. P. Byrne, G. D. Dracoulis, T. Kibédi, T. R. McGoram, and S. M. Mullins, Nucl. Phys. A **691**, 577 (2001).
[4] E. Grodner *et al.*, Int. J. Mod. Phys. E **14**, 347 (2005).
[5] E. Grodner, J. Srebrny, A. A. Pasternak, I. Zalewska, T. Morek, C. Droste, J. Mierzejewski, M. Kowalczyk, J. Kownacki *et al.*, Phys. Rev. Lett. **97**, 172501 (2006).
[6] E. Grodner *et al.*, Int. J. Mod. Phys. E **15**, 548 (2006).
[7] D. J. Hartley, L. L. Riedinger, M. A. Riley, D. L. Balabanski, F. G. Kondev, R. W. Laird, J. Pfohl, D. E. Archer, T. B. Brown *et al.*, Phys. Rev. C **64**, 031304(R) (2001).
[8] A. A. Hecht, C. W. Beausang, K. E. Zyromski, D. L. Balabanski, C. J. Barton, M. A. Caprio, R. F. Casten, J. R. Cooper, D. J. Hartley *et al.*, Phys. Rev. C **63**, 051302(R) (2001).
[9] A. A. Hecht, C. W. Beausang, H. Amro, C. J. Barton, Z. Berant, M. A. Caprio, R. F. Casten, J. R. Cooper, D. J. Hartley *et al.*, Phys. Rev. C **68**, 054310 (2003).
[10] P. Joshi *et al.*, Phys. Lett. B **595**, 135 (2004).
[11] P. Joshi *et al.*, J. Phys. G: Nucl. Part. Phys. **31**, S1895 (2005).
[12] P. Joshi *et al.*, Eur. Phys. J. A **24**, 23 (2005).
[13] P. Joshi, M. P. Carpenter, D. B. Fossan, T. Koike, E. S. Paul, G. Rainovski, K. Starosta, C. Vaman, and R. Wadsworth, Phys. Rev. Lett. **98**, 102501 (2007).
[14] T. Koike, K. Starosta, C. J. Chiara, D. B. Fossan, and D. R. LaFosse, Phys. Rev. C **63**, 061304(R) (2001).
[15] T. Koike, K. Starosta, C. J. Chiara, D. B. Fossan, and D. R. LaFosse, Phys. Rev. C **67**, 044319 (2003).
[16] T. Koike, K. Starosta, and I. Hamamoto, Phys. Rev. Lett. **93**, 172502 (2004).
[17] E. A. Lawrie, P. A. Vymers, J. J. Lawrie, C. Vieu, R. A. Bark, R. Lindsay, G. K. Mabala, S. M. Maliage, P. L. Masiteng *et al.*, Phys. Rev. C **78**, 021305(R) (2008).
[18] E. A. Lawrie *et al.*, Eur. Phys. J. A **45**, 39 (2010).
[19] E. O. Lieder, R. M. Lieder, R. A. Bark, Q. B. Chen, S. Q. Zhang, J. Meng, E. A. Lawrie, J. J. Lawrie, S. P. Bvumbi *et al.*, Phys. Rev. Lett. **112**, 202502 (2014).
[20] Y. X. Luo *et al.*, Phys. Lett. B **670**, 307 (2009).
[21] Y. X. Luo *et al.*, Phys. Lett. B **691**, 285(E) (2010).
[22] P. L. Masiteng *et al.*, Acta Phys. Pol. B **40**, 657 (2009).
[23] P. L. Masiteng *et al.*, Phys. Lett. B **719**, 83 (2013).
[24] P. L. Masiteng *et al.*, Eur. Phys. J. A **50**, 119 (2014).
[25] P. L. Masiteng *et al.*, Eur. Phys. J. A **52**, 28 (2016).
[26] E. Mergel *et al.*, Eur. Phys. J. A **15**, 417 (2002).
[27] C. B. Moon, T. Komatsubara, and K. Furuno, Nucl. Phys. A **674**, 343 (2000).
[28] C. B. Moon, T. Komatsubara, and K. Furuno, Nucl. Phys. A **678**, 457 (2000).
[29] S. Mukhopadhyay, D. Almehed, U. Garg, S. Frauendorf, T. Li, P. V. Madhusudhana Rao, X. Wang, S. S. Ghughre, M. P. Carpenter, S. Gros, A. Hecht, R. V. F. Janssens, F. G. Kondev, T. Lauritsen, D. Seweryniak, and S. Zhu, Phys. Rev. Lett. **99**, 172501 (2007).
[30] S. Mukhopadhyay, D. Almehed, U. Garg, S. Frauendorf, T. Li, P. V. Madhusudhana Rao, X. Wang, S. S. Ghugre, M. P. Carpenter, S. Gros, A. Hecht, R. V. F. Janssens, F. G. Kondev, T. Lauritsen, D. Seweryniak, and S. Zhu, Phys. Rev. C **78**, 034311 (2008).
[31] C. M. Petrache *et al.*, Phys. Rev. C **65**, 054324 (2002).
[32] C. M. Petrache *et al.*, Nucl. Phys. A **597**, 106 (1996).
[33] G. Rainovski *et al.*, J. Phys. G: Nucl. Part. Phys. **29**, 2763 (2003).
[34] G. Rainovski, E. S. Paul, H. J. Chantler, P. J. Nolan, D. G. Jenkins, R. Wadsworth, P. Raddon, A. Simons, D. B. Fossan *et al.*, Phys. Rev. C **68**, 024318 (2003).
[35] A. J. Simons *et al.*, J. Phys. G: Nucl. Part. Phys. **31**, 541 (2005).
[36] K. Starosta, C. J. Chiara, D. B. Fossan, T. Koike, T. T. S. Kuo, D. R. LaFosse, S. G. Rohoziński, Ch. Droste, T. Morek, and J. Srebrny, Phys. Rev. C **65**, 044328 (2002).
[37] T. Suzuki, G. Rainovski, T. Koike, T. Ahn, M. P. Carpenter, A. Costin, M. Danchev, A. Dewald, R. V. F. Janssens *et al.*, Phys. Rev. C **78**, 031302(R) (2008).
[38] J. Timár *et al.*, Phys. Lett. B **598**, 178 (2004).
[39] J. Timár *et al.*, Phys. Rev. C **76**, 024307 (2007).
[40] D. Tonev, M. S. Yavahchova, N. Goutev, G. deAngelis, P. Petkov, R. K. Bhowmik, R. P. Singh, S. Muralithar, N. Madhavan *et al.*, Phys. Rev. Lett. **112**, 052501 (2014).
[41] D. Tonev, G. deAngelis, P. Petkov, A. Dewald, S. Brant, S. Frauendorf, D. L. Balabanski, P. Pejovic, D. Bazzacco *et al.*, Phys. Rev. Lett. **96**, 052501 (2006).
[42] D. Tonev, G. de Angelis, S. Brant, S. Frauendorf, P. Petkov, A. Dewald, F. Dönau, D. L. Balabanski, Q. Zhong, P. Pejovic, D. Bazzacco, P. Bednarczyk, F. Camera, D. Curien, F. Della Vedova, A. Fitzler, A. Gadea, G. Lo Bianco, S. Lenzi, S. Lunardi, N. Marginean, O. Moller, D. R. Napoli, R. Orlandi, E. Sahin, A. Saltarelli, J. Valiente Dobon, K. O. Zell, J. Y. Zhang, and Y. H. Zhang, Phys. Rev. C **76**, 044313 (2007).
[43] C. Vaman, D. B. Fossan, T. Koike, K. Starosta, I. Y. Lee, and A. O. Macchiavelli, Phys. Rev. Lett. **92**, 032501 (2004).
[44] S. Wang, Y. Liu, T. Komatsubara, Y. Ma, and Y. Zhang, Phys. Rev. C **74**, 017302 (2006).
[45] J. Yong-Nam *et al.*, J. Phys. G: Nucl. Part. Phys. **31**, B1 (2005).
[46] S. Zhu *et al.*, Phys. Rev. Lett. **91**, 132501 (2003).
[47] S. J. Zhu *et al.*, Eur. Phys. J. A **25**, 459 (2005).
[48] B. Moon *et al.*, Phys. Lett. B **782**, 602 (2018).
[49] M. Wang, Y. Y. Wang, L. H. Zhu, B. H. Sun, G. L. Zhang, L. C. He, W. W. Qu, F. Wang, T. F. Wang *et al.*, Phys. Rev. C **98**, 014304 (2018).
[50] K. Selvakumar, A. K. Singh, C. Ghosh, P. Singh, A. Goswami, R. Raut, A. Mukherjee, U. Datta, P. Datta *et al.*, Phys. Rev. C **92**, 064307 (2015).
[51] C. M. Petrache, Q. B. Chen, S. Guo, A. D. Ayangeakaa, U. Garg, J. T. Matta, B. K. Nayak, D. Patel, J. Meng *et al.*, Phys. Rev. C **94**, 064309 (2016).
[52] K. Y. Ma *et al.*, Phys. Rev. C **97**, 014305 (2018).
[53] T. Roy *et al.*, Phys. Lett. B **782**, 768 (2018).
[54] J. Meng, J. Peng, S. Q. Zhang, and S. G. Zhou, Phys. Rev. C **73**, 037303 (2006).
[55] J. Peng, H. Sagawa, S. Q. Zhang, J. M. Yao, Y. Zhang, and J. Meng, Phys. Rev. C **77**, 024309 (2008).
[56] J. M. Yao, B. Qi, S. Q. Zhang, J. Peng, S. Y. Wang, and J. Meng, Phys. Rev. C **79**, 067302 (2009).
[57] J. Li, S. Q. Zhang, and J. Meng, Phys. Rev. C **83**, 037301 (2011).
[58] P. W. Zhao, Phys. Lett. B **773**, 1 (2017).
[59] Q. B. Chen, B. F. Lv, C. M. Petrache, and J. Meng, Phys. Lett. B **782**, 744 (2018).

[60] J. Peng and Q. B. Chen, Phys. Rev. C **98**, 024320 (2018).
[61] J. Li, Phys. Rev. C **97**, 034306 (2018).
[62] B. Qi, H. Jia, C. Liu, and S. Y. Wang, Phys. Rev. C **98**, 014305 (2018).
[63] A. D. Ayangeakaa, U. Garg, M. D. Anthony, S. Frauendorf, J. T. Matta, B. K. Nayak, D. Patel, Q. B. Chen, S. Q. Zhang, P. W. Zhao, B. Qi *et al.*, Phys. Rev. Lett. **110**, 172504 (2013).
[64] I. Kuti *et al.*, Phys. Rev. Lett. **113**, 032501 (2014).
[65] B. F. Lv, C. M. Petrache, A. Astier, E. Dupont, A. Lopez-Martens, P. T. Greenlees, H. Badran, T. Calverley, D. M. Cox *et al.*, Phys. Rev. C **98**, 044304 (2018).
[66] C. M. Petrache, B. F. Lv, A. Astier, E. Dupont, Y. K. Wang, S. Q. Zhang, P. W. Zhao, Z. X. Ren, J. Meng *et al.*, Phys. Rev. C **97**, 041304(R) (2018).
[67] C. Liu, S. Y. Wang, R. A. Bark, S. Q. Zhang, J. Meng, B. Qi, P. Jones, S. M. Wyngaardt, J. Zhao *et al.*, Phys. Rev. Lett. **116**, 112501 (2016).
[68] J. Ndayishimye, Ph.D. thesis, University of Stellenbosch, Cape Town, South Africa, 2016.
[69] J. Ndayishimye *et al.*, Acta Phys. Pol. B **48**, 343 (2017).
[70] E. A. Lawrie, Phys. Scr. **92**, 094006 (2017).
[71] E. A. Lawrie, J. Ndayishimye, P. L. Masiteng, and O. Shirinda, Acta Phys. Pol. B Proc. Suppl. **11**, 81 (2018).
[72] http://www.xia.com.
[73] D. Radford, Nucl. Instrum. Methods A **361**, 297 (1995).
[74] T. Yamazaki, Nucl. Data **3**, 1 (1967).
[75] W. Reviol *et al.*, Nucl. Phys. A **548**, 331 (1992).
[76] O. Shirinda and E. A. Lawrie, Eur. Phys. J. A **52**, 344 (2016).
[77] H. Hübel, A. P. Byrne, S. Ogaza, A. E. Stuchbery, G. D. Dracoulis, and M. Guttormsen, Nucl. Phys. A **453**, 316 (1986).
[78] E. Gueorguieva *et al.*, Phys. Rev. C **68**, 054308 (2003).
[79] F. G. Kondev, S. Juutinen, and D. J. Hartley, Nucl. Data Sheets **150**, 1 (2018).
[80] T. D. Johnson and B. Singh, Nucl. Data Sheets **142**, 1 (2017).
[81] B. Singh, Nucl. Data Sheets **99**, 275 (2003).
[82] V. R. Vanin, N. L. Maidana, R. M. Castro, E. Achterberg, O. A. Capurro, and G. V. Marté, Nucl. Data Sheets **108**, 2393 (2007).
[83] Coral M. Baglin, Nucl. Data Sheets **113**, 1871 (2012).
[84] B. Singh, Nucl. Data Sheets **107**, 1531 (2006).
[85] T. Bengtsson and I. Ragnarsson, Nucl. Phys. A **436**, 14 (1985).
[86] B. G. Carlsson and I. Ragnarsson, Phys. Rev. C **74**, 011302(R) (2006).
[87] H. Hübel, A. P. Byrne, S. Ogaza, A. E. Stuchbery, and M. Guttormsen, Phys. Lett. B **145**, 29 (1984).